Molecular Dynamics Simulation of Syndio- and Isotactic Poly(methyl methacrylate) in Benzene

U. M. Apel, R. Hentschke,* and J. Helfrich

Max-Planck-Institut für Polymerforschung, Postfach 3148, 55021 Mainz, Germany

Received September 13, 1994; Revised Manuscript Received December 16, 1994[⊗]

ABSTRACT: We carry out molecular dynamics simulations of syndio- and isotactic poly(methyl methacrylate) (PMMA) using explicit benzene as solvent. Experiments show that the tacticity of PMMA strongly influences the q-dependence of the scattering intensity. Here we calculate X-ray scattering intensities of high molecular weight fragments constructed from simulation trajectories. We compare these results with experimental measurements as well as other theoretical models based on the rotational isomeric state approach. Furthermore, we analyze the conformational scaling behavior and the solvation shell structure.

Introduction

In this work we apply the molecular dynamics (MD) simulation technique to oligomers of syndiotactic (s-) and isotactic (i-) PMMA dissolved in benzene. The simulations are carried out using the AMBER (Assisted Model Building with Energy Refinement) force field employing the standard force field parameters,[1,2] where both solute and solvent are included explicitly on the level of the individual atoms. On the basis of the simulated conformations of syndio- and isotactic 16-mers, we construct high molecular weight fragments according to a method discussed previously.[3] This method of constructing high molecular weight fragments via smoothly chaining time-uncorrelated oligomeric segments was tested for poly(γ-benzyl L-glutamate) (PBLG) in dimethylformamide (DMF),[3] where it predicts the persistence length in excellent accord with the experiment. Thus, in the present case the conformations of the constructed high molecular weight fragments should closely correspond to conformations of the real polymer in dilute solution, with benzene as solvent. Here we first study the dependence of the chain conformation on the degree of polymerization in terms of the characteristic ratio for s- and i-PMMA in benzene. For short distances ($\lesssim$25 monomers) our results are in good accord with previous rotational isomeric state (RIS) calculations of Vacatello and Flory.[4] For larger distances we observe and discuss significant deviations. As a more stringent test of the simulation, however, we calculate the X-ray scattering intensity based on the simulated high molecular weight fragments, which is then compared to the experimental data of Wunderlich and Kirste[5] and Yamaguchi et al.[6] Using the atomic group form factors obtained in ref 6, we find quite good qualitative agreement with the experiment for the case of s-PMMA, comparable to the six-state transfer matrix calculations of Vacatello and Flory[4] over the entire experimental range of the scattering vector. In particular, our simulation reproduces the two maxima at $q = 0.10$ and 0.55 Å^{-1} observed in the experiment. The agreement for the case of i-PMMA is not so good. This is somewhat surprising, because of the rather featureless form of the experimental Kratky curves. However, we find that here the agreement with the experimental data can be improved by constructing quasi-atactic high molecular weight fragments, which contain syndio- and isotactic sequences in varying proportion. Finally, we also investigate the solvation shell structure for the two cases. We find that s-PMMA exhibits a comparatively more structured solvation shell, extending out to 12 Å away from the C_α and O_{ester} atoms.

Initial Oligomer Conformations and the Construction of the Simulation Box

The time necessary to attain conformational equilibrium during the simulation is significantly influenced by the choice of the initial oligomer conformations. This is of particular importance for molecular dynamic simulations, where the inclusion of atomic detail and the attendant numerical effort induces severe time constraints. For PMMA, as we show below, we may take the solid-state conformations as reasonable starting conformations for short oligomers in solution.

Crystallization of s-PMMA is induced by solvent treatment,[7] where the solvent is necessary for maintaining the crystallinity. After inducing the crystallization with chloroacetone, this initiator may be substituted by another solvent, for example, benzene.[8] X-ray investigations show that s-PMMA forms isomorphous crystalline inclusion complexes with these solvents. Within these complexes s-PMMA forms a helix consisting of 74 monomeric units with a repeat distance of 35.4 Å,[8] where the backbone conformation is close to the all-trans conformation. For this reason and because there is no detailed crystal information available we choose an all-trans conformation as the s-PMMA starting structure.

X-ray experiments on i-PMMA show that the crystalline solid-state conformation of lowest energy is a helix. Whereas the experimental scattering pattern allows more than one probable helix model, some of these models are ruled out by additional infrared studies and conformational energy analysis.[9–12] Here we have analyzed Tadokoro's suggestions for two 5/1, one 5/2, and one 10/1 helix[9,11] (in the crystalline state the 10/1 helix occurs as a double helix) via static energy minimization with the POLYGRAF software package.[13] We find the 10/1 helix to be the one with the lowest energy in agreement with ref 11. Thus here we adopt the 10/1 helix as the initial conformation for the i-PMMA oligomer.

The s- and i-PMMA oligomers used in the MD simulations described below consist of 16 monomer units terminated by a methyl group (cf. Figure 1). Following a procedure described previously[3,14] each oligomer is inserted in a simulation box of volume $V = L^3$ (=(32 Å)^3) filled with benzene preequilibrated at $T = 300$ K,

[⊗] Abstract published in *Advance ACS Abstracts,* February 1, 1995.

0024-9297/95/2228-1778$09.00/0

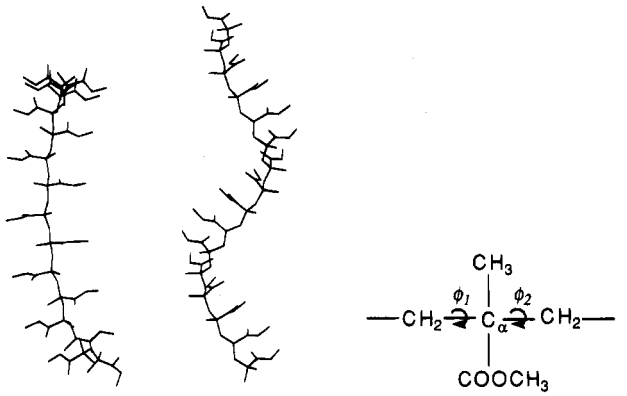

Figure 1. Initial conformations of the two oligomers (consisting of 16 monomers each) used in the simulation. The sketch on the right explains our convention for the dihedral angles.

where overlapping solvent molecules are deleted. The molecules are treated without any simplification, that is, in the all-atom description. This leads to a total of 2501 atoms for the case of s-PMMA and to 2525 atoms for the case of i-PMMA, respectively. Notice that the number of deleted solvent molecules upon insertion depends on the tacticity of the inserted oligomer.

Simulation Methodology

In MD simulations the phase space is sampled by integrating numerically Newton's equations of motion

$$m_i = \frac{d^2\vec{x}_i}{dt^2} = -\vec{\nabla}_{\vec{x}_i} V(\vec{x}_1,...,\vec{x}_n) \quad (1)$$

for every atom i contained in the simulation box. Here we carrry out our simulations using the molecular mechanics and molecular dynamics modules provided in the AMBER molecular modeling packaging. In the present case the AMBER potential $V(\vec{x}_1,...,\vec{x}_n)$ is

$$V = \sum_{\text{bonds}} f_r (r - r_{\text{equ}})^2 + \sum_{\substack{\text{valence}\\ \text{angles}}} f_\delta (\delta - \delta_{\text{equ}})^2 + \sum_{\text{dihedrals}} f_n (1 + \cos(n\phi - \gamma)) + \sum_{i<j}\left(\frac{A_{ij}}{r_{ij}^{12}} - \frac{B_{ij}}{r_{ij}^{6}}\right) + \sum_{i<j}\frac{q_i q_j}{r_{ij}} \quad (2)$$

$$A_{ij} = (\epsilon_i \epsilon_j)^{1/2}(\sigma_i + \sigma_j)^{12}$$

$$B_{ij} = 2(\epsilon_i \epsilon_j)^{1/2}(\sigma\sigma_j)^6$$

The first three terms describe the bonding interactions, which include harmonic bond stretch and valence angle potentials as well as a cosine-type potential for the dihedral rotations. The last two terms represent the nonbonding Lennard-Jones and Coulomb interactions. Here we apply the Lorentz–Berthelot mixing rule[15] to obtain the usual LJ parameters ϵ_{ij} and σ_{ij}, i.e., $\epsilon_{ij} = (\epsilon_i\epsilon_j)^{1/2}$ and $\sigma_{ij} = \sigma_i + \sigma_j$, where σ_i and σ_j include a factor 0.5. Notice also that all 1–4 nonbonded interactions (LJ and Coulomb interactions between atoms separated by three bonds) are scaled by a factor 0.5.[1,2] The potential parameters with the exception of the atomic partial charges are taken from the AMBER data base[1,2] and from ref 16. The partial charges of PMMA are calculated using the charge equilibration method[17] included in the POLYGRAF software package;[13] the partial charges of benzene are taken from ref 18. All potential parameters including the partial charges are compiled in Table 1.

Table 1. All Force Field Parameters, Which Are Extracted from the AMBER Data Base[1,2] if the Source Is Not Referenced Separately[a]

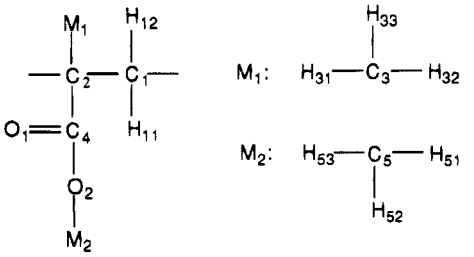

bonds	f_r (kcal mol^{-1} Å^{-2})	r_{equ} (Å)	ref
C–CT	317	1.52	
C–O	570	1.23	
CT–CT	310	1.53	
CT–HC	331	1.09	
CT–OS	320	1.41	
C–OS	214	1.33	16
C–CA	469	1.40	
CA–HC	340	1.08	

angles	f_δ (kcal mol^{-1})	δ_{equ} (deg)	ref
CT–C–O	80	120.4	
C–CT–CT	63	111.10	
CT–CT–CT	40	109.5	
CT–CT–HC	35	109.5	
HC–CT–HC	35	109.5	
C–OS–CT	83	116.9	16
O–C–OS	83	123.4	16
OS–C–CT	81	111.4	16
CA–CA–CA	35	120.0	
CA–CA–HC	35	120.0	

dihedral angles	f_n (kcal mol^{-1})	γ (deg)	n	ref
X–C–CT–X	0.00	0.00	6	
X–CT–CT–X	1.3	0.00	9	
X–CT–OS–X	1.15	0.00	3	
CT–CT–C–O	0.07	180.00	1	
CT–C–OS–CT	5.09	0.00	1	
O–C–OS–CT	8.30	180.00	1	
X–CA–CA–X	5.30	180.00	4	
X–X–CA–HC	2.0	180.00	1	

LJ parameters	ϵ (kcal mol^{-1})	σ (Å)
C	0.12	1.85
CA	0.12	1.85
CT	0.06	1.80
HC	0.01	1.54
OS	0.15	1.65
O	0.20	1.60

partial charges	q (electron charges)	partial charges	q (electron charges)
C_1	−0.24	C_4	0.67
H_{11}	0.18	O_1	−0.55
H_{12}	0.11	O_2	−0.60
C_2	0.02	C_5	−0.09
C_3	−0.35	H_{51}	0.13
H_{31}	0.19	H_{52}	0.11
H_{32}	0.14	H_{53}	0.17
C(benzene)	−0.15	H(benzene)	0.15

[a] We use the AMBER atom type convention: C = carbonyl carbon, CA = aromatic carbon in a six-membered ring with one substituent, CT = carbon with four explicit substituents, HC = explicit hydrogen attached to carbon, O = carbonyl oxygen, OS = ethyl and ester oxygen. The partial charges are calculated via the charge equilibration algorithm,[17] which is part of the POLYGRAF modeling package.[13] Note that the partial charges for the head and tail monomer differ slightly from those indicated.

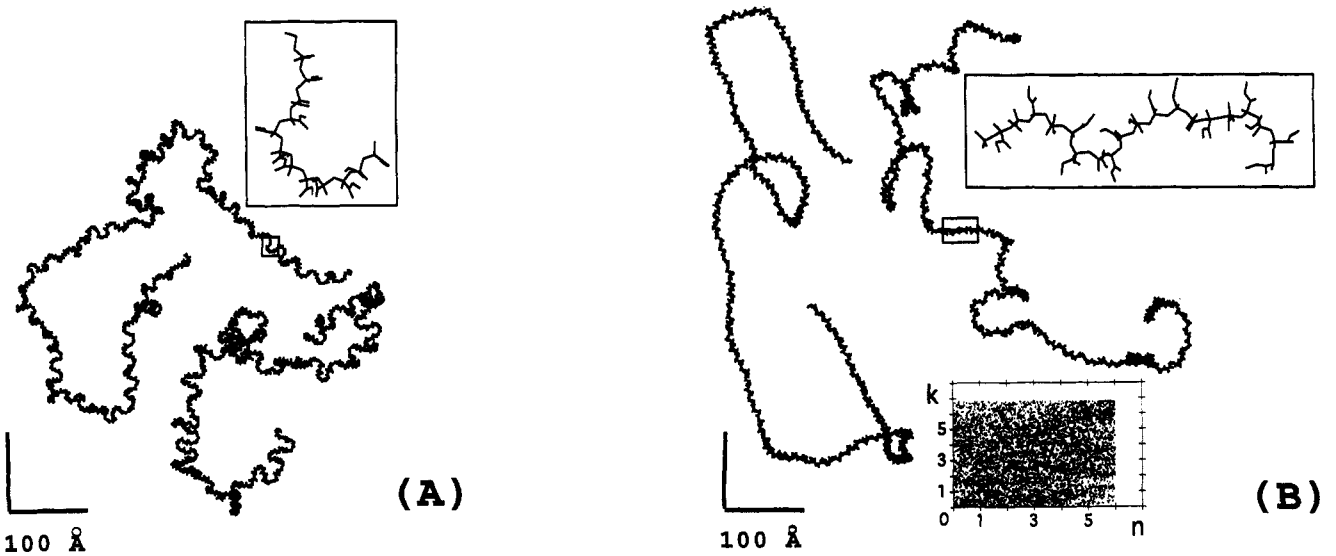

Figure 2. Two syndiotactic (A) and two isotactic (B) PMMA high molecular weight fragments constructed from the oligomer simulation trajectories according to the procedure described in the text. The boxes show enlarged chain segments (scale factor = 10). The additional inset within B illustrates the quasi random relation between the position k of an oligomer in the conformation list and its position n within one of the isotactic high molecular weight fragments shown in this figure (both k and n are in units of 1000).

The dynamic simulations are preceded by a static energy minimization of the entire simulation box in order to relax possible van der Waals overlaps. To limit the number of nonbonded interactions, and thus the numerical effort, a residue based cutoff of 8 Å is used throughout the energy minimization as well as during the subsequent MD simulations. Notice that here each benzene and each monomer unit within the oligomer constitutes a residue and that all nonbonded interactions are calculated between two residues, if the smallest atom-to-atom distance between the two residues is less than 8 Å. The numerical integration of the equations of motion is carried out using a leap-frog version of the Verlet–Strömer algorithm with a 1.0 fs time step. Furthermore, we employ periodic boundary conditions as well as the minimum image convention. Our MD simulations are performed within the *NVT* ensemble; i.e., particle number, volume, and temperature are kept constant, where $T = 300$ K. Constant temperature is maintained according to the method of Berendsen et al.[19] using velocity scaling with a temperature relaxation time of 0.1 ps. The scattering results reported below are based on 700 ps simulation runs for each tacticity of which we discard the first 20 ps.

Construction of Syndiotactic and Isotactic High Molecular Weight Fragments

The simulations are carried out for oligomers containing 16 monomer units. On the other hand, the experimental scattering results, which we want to compare to, are for dilute solutions containing polymers with a molecular weight corresponding to about 2000–3000 monomer units. In this section we describe a formalism, which allows us to construct high molecular weight fragments of corresponding size, based on statistically independent conformations extracted from the trajectories of the 16-mers. The resulting chains should closely mimic the single chain behavior of s- and i-PMMA in benzene.

The procedure, which we have recently tested for PBLG in DMF,[3] is as follows. First, we create a list containing instantaneous conformations of the simulated oligomer, which are extracted from the simulation trajectory at regular time intervals Δt, where here $\Delta t = 0.1$ ps. Next, assuming that a chain (s- or i-PMMA) consisting of n connected oligomers already exists, we want to "smoothly" extend this chain by an additional oligomer conformation taken from the above list of conformations. Thus, we scan the list of oligomers for the best match between the tail backbone dihedral angle $\phi_{2,t}$ of the already existing chain and the head backbone dihedral angle $\phi_{2,h}$ of the oligomers in the list (cf. Figure 1). The oligomer for which $|\phi_{2,t} - \phi_{2,h}|$ has a minimum is then connected (as the $(n + 1)$st oligomer) to the chain, and, simultaneously, it is deleted from the list. Notice also that when the oligomer is connected to the chain the overlapping tail monomer of the chain is deleted. This process is then repeated. Figure 2 shows four high molecular weight fragments (two for s-PMMA and two for i-PMMA) each containing 1000 monomers, which are constructed in this fashion. Notice that the s-PMMA segments appear to be more strongly coiled, exhibiting, for instance, pronounced loops on a scale of about 15 Å up to 50 Å. Using one of two isotactic high molecular weight fragments as an example, the inset in Figure 2B illustrates the quasi randomness between the position k of an oligomer in the conformation list and its position n within the high molecular weight fragment.

At this point it is useful to address some details of the above construction procedure. Our oligomers consist of 16 PMMA monomers. This leads to a sequence of 15 dihedral angles ϕ_2 (cf. Figure 1) for every oligomer. Due to the above connection rule, we then have a maximum number of 14 dihedral angles ϕ_2 per oligomer conformation added to a chain. Of course, we also can build high molecular weight fragments connecting oligomer segments containing less than 14 dihedral angles ϕ_2. Note that for each of these cases there exist several choices for selecting the corresponding oligomer segment. For instance, an additional segment containing 13 dihedral angles ϕ_2 can be selected by matching ϕ_2 of the 15th (14th) monomer of the nth oligomer conformation in the chain to ϕ_2 of the 2nd (1st) monomer in the oligomer conformation to be added as the $(n + 1)$st segment. Thus here different kinds of chains are built, based on the

same pool of oligomer conformations. However, each kind is composed of segments of the same length, where the maximum is 14 monomers and the minimum is 7 monomers. In addition, we exclude all chains or high molecular weight fragments containing "bad choices"; i.e., the minimum of $|\phi_{2,t} - \phi_{2,h}|$ involves dihedral angles $\phi_{2,t}$ and $\phi_{2,h}$, whose corresponding distributions do not overlap. This overlap condition leads to 9 different syndiotactic and 25 different isotactic chain types. Note that in the case of s-PMMA some combinations of head and tail monomers are excluded in order to preserve syndiotacticity, which reduces the possible number of chain types for s-PMMA. Finally, for each type of chain we create a certain number (cf. below) of high molecular weight fragments over which we average. This construction and averaging procedure also diminishes possible end effects, i.e., effects due to including dihedral angles close to the free ends of the simulated oligomers. We have attempted to study these end effects quantitatively by systematically excluding end dihedral angles. However, the results obtained in this fashion are not significantly different from those obtained via the above overall average.

The construction procedure, as it stands, neglects excluded volume beyond the oligomer segments, which make up the high molecular weight fragments. Of course the chain excluded volume might be included via an additional "no-overlap" condition applied to the atom–atom separations within each high molecular weight fragment. We have calculated the number of chain self-interactions using a minimum atom–atom distance of 2 Å. Within the s-PMMA chains there are virtually no overlaps within the first 20 monomer units. After that we find a pronounced maximum at ≈35 monomers and subsequent diminishing maxima every ≈30 monomers, indicating a looplike structure on this length scale (30 monomers ≈ 75 Å). For i-PMMA there is a small number of overlaps at the segment joints due to overlapping side chains. Again there is a maximum at 30 monomer units (the maximum is, however, significantly smaller than that for the s-PMMA chains) but no subsequent maxima. In the following we do not exclude intersecting chains from the analysis. This is because we are mainly interested in the short distance behavior on length scales of several tens of monomers. Also, the quantitative evaluation of effects due to long-range chain–chain exclusion is difficult, because the relative rarity of chain–chain intersections makes longer trajectories than the ones which we have available in the present case necessary. Moreover, the above overlap criterion is purely geometric and does not model the solvent specificity of the chain–chain interactions. Finally, it is worth noting that we are also interested in comparing to the rotational isomeric state (RIS) model results where likewise the long-range chain–chain exclusion is omitted. Comparing to the experimental results, however, we must except deviations when length scales larger than ≈30 monomer units are considered.

Chain Conformations and Scattering Functions for s- and i-PMMA High Molecular Weight Fragments

The construction procedure of the previous section allows one to study the dependence of the solution behavior of s- and i-PMMA in benzene on the number of chain monomers N. Figure 3 shows a plot of the mean-square end-to-end separation $\langle R_{2N}^2 \rangle$ divided by $2l^2N$ vs $1/N$, where $l = 1.53$ Å is the C–C bond length along the backbone. For the unperturbed R_{2N} the quantity $\langle R_{2N}^2 \rangle/(2l^2N)$ is the characteristic ratio C_{2N}, which not only is a function of intrinsic chain properties but also depends on the polymer–solvent interaction. The high molecular weight fragments considered here contain 8400 monomers, and we build five polymers for each chain type. So the average is taken over 45 and 125 chains for s- and i-PMMA, respectively. In the range $0.04 \lesssim 1/N \lesssim 0.2$ the MD results are in qualitative accord with the six-state RIS results of Vacatello and Flory;[4] i.e., we also observe a maximum for s-PMMA, whereas for i-PMMA we obtain a monotonous increase. In addition, we also find the crossover between s- and i-PMMA at about 0.1. Vacatello and Flory attribute the occurrence of the maximum of C_{2N} for s-PMMA to the circling back of the chain onto itself. Our local maximum of C_{2N} for s-PMMA occurs at $N \simeq 17$, which almost exactly is half of the N for which we obtain the first maximum in the overlap distribution discussed in the previous section. Nevertheless, if we take 2.54 Å to be the length of a monomer along the chain contour, then our local maximum of C_{2N} occurs at ~42 Å, which is a length scale on which we do indeed see strong coiling of the s-PMMA chains (cf. Figure 2). In the range $1/N < 0.04$ the MD simulation yields a significantly larger C_{2N} than the RIS calculation. In fact, the values for C_∞ which we obtain are 45 ± 5 for s- and 72 ± 5 for i-PMMA (not shown in Figure 3). Whereas their ratio is in rough agreement with the corresponding result in ref 4 (cf. also Figure 3), our absolute numbers do exceed these values by a factor of ~7! We are not aware of measured values for C_{2N} for either s-PMMA or i-PMMA in benzene. However, the experimental results, which are obtained by, for example, measuring the perturbed chain dimen-

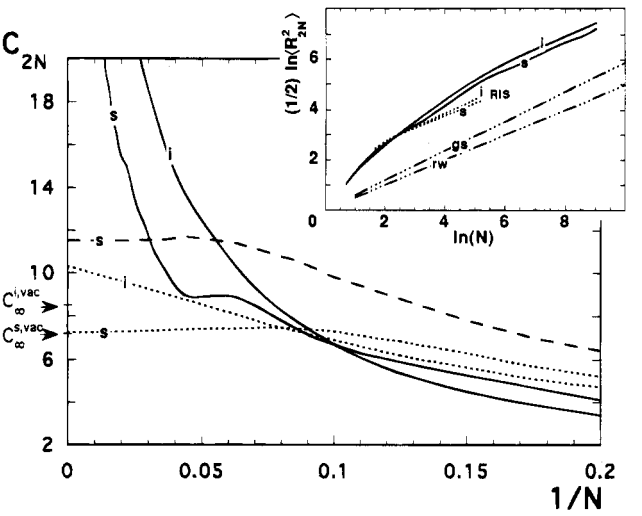

Figure 3. Characteristic ratio $C_{2N} = \langle R_{2N}^2 \rangle/(2Nl^2)$ vs the inverse number of monomers $1/N$ for both s- and i-PMMA. Here $\langle R_{2N}^2 \rangle$ is the mean-square end-to-end distance and $l = 1.53$ Å is the C–C bond length along the backbone. The solid lines are the simulation results for s- and i-PMMA in benzene. The short-dashed lines show the corresponding vacuum six-state RIS results taken from ref 4, and the long-dashed line shows the 14-state RIS results for s-PMMA taken from ref 6. The arrows on the left show the results for C_∞ for s- and i-PMMA vacuum simulations. Inset: The logarithm of the mean-square end-to-end distance R_{2N} divided by 2 vs the logarithm of the number of monomers N. Long solid lines: simulation results for s- and i-PMMA. Short-dashed lines: six-state RIS model results for s- and i-PMMA as in the main panel. Dash-dotted lines: scaling behavior, i.e., $\langle R_{2N}^2 \rangle \approx N^{2\nu}$, for a polymer chain in a good solvent (gs: $\nu = 0.6$) and the simple random-walk result (rw: $\nu = 0.5$),[29] plotted for an effective segment of length unity.

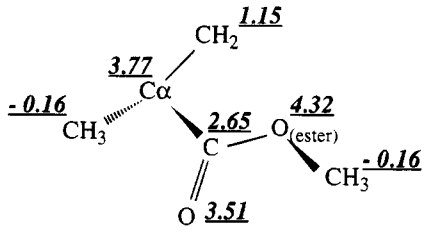

Figure 4. Excess form factors f_i of the various atom groups within the PMMA monomer taken from ref 6.

sions and then extracting the unperturbed dimensions according to different semiempirical theoretical models,[20,21] yield values for C_∞ which vary depending on tacticity and solvent roughly between 6 and 11.[20,22-28] In order to check our procedure, we therefore performed additional analogous reference simulations in vacuum instead of in benzene. The resulting values for C_∞ are 7.2 ± 0.3 for s-PMMA and 8.5 ± 1.1 for i-PMMA (indicated by the arrows in Figure 3). These values are in quite good agreement with the (vacuum) six-state RIS results in ref 4. Thus, the discrepancy should be due to explicitly including the solvent. Benzene is considered to be a good solvent,[23] which means that $\langle R_{2N}^2 \rangle$ should scale as $N^{2\nu}$ with $\nu \approx 0.6$[29] for large N. Because, however, we do not include excluded-volume interactions beyond the length of the oligomers (cf. above), our $\langle R_{2N}^2 \rangle$ must eventually scale with $\nu = 1/2$, as shown in the inset in Figure 3. Nevertheless, a PMMA segment stiffened by the surrounding solvation shell, which is discussed below, forms a rather bulky object for which l may not be a meaningful length in this context;[21] i.e., l should be replaced by a much larger effective "bond" length (cf. the inset in Figure 3). One additional source of error, which we want to mention in this context, is the finite size of the simulation box, which means that there are possible interactions between the polymer segment and its images leading to the stiffening of the segments. Even though the direct segment–segment interaction is avoided by the employed interaction cutoff, interactions between the real and the image solvation shells cannot be ruled out completely. A systematic investigation of this point would require several reference simulations for different box sizes, which computationally is very expensive.

A better check for the respective qualities of the simulation and the RIS predictions, however, is the comparison to experimental X-ray scattering results obtained on dilute solutions of s- and i-PMMA in benzene. For the above high molecular weight fragments of s- and i-PMMA we calculate the scattering function

$$F(q) = \frac{1}{N^2(\sum' f_i)^2} \sum_{ij}' \left\langle f_i f_j \frac{\sin(qr_{ij})}{qr_{ij}} \right\rangle \qquad (3)$$

for a system of independent randomly oriented molecules consisting of N monomers each. Here r_{ij} is the separation between two scattering sites labeled by i and j, and q is the magnitude of the scattering vector given by $q = (4\pi/\lambda)\sin(\theta/2)$, where $\lambda = 1.54$ Å and θ is the scattering angle. The f_i are the excess form factors of the atoms (or atom groups) shown in Figure 4 for a single monomer unit, which are calculated according to the equation

$$f_i = f_i^0 - \varrho V_i \qquad (4)$$

The f_i^0 are the bare form factors taken to be equal to the charge number of the atom (or atom group) at the scattering site i, which is a good approximation in the q-range studied here. The term ϱV_i is the excluded solvent electron charge, where ϱ is on its van der Waals volume and the partial specific volume. The details of this calculation are given in ref 6, but the resulting values for f_i are shown in Figure 4. Notice also that the primed summation in the denominator of eq 3 is carried out over the scattering sites within one monomer unit only. Thus, for monomer–monomer contributions to $F(q)$ from distant sites (relative to the size of a monomer unit) separated by r, we can write $r_{ij} \approx r$ and carry out the intramonomer summation over $f_i f_j$ independently, so that $F(q)$ is independent of the f_i for small q. Finally, the average in eq 3 is over 180 high molecular weight fragments in the case of s-PMMA and 500 high molecular weight fragments in the case of i-PMMA, where each fragment consists of 2000 monomers.

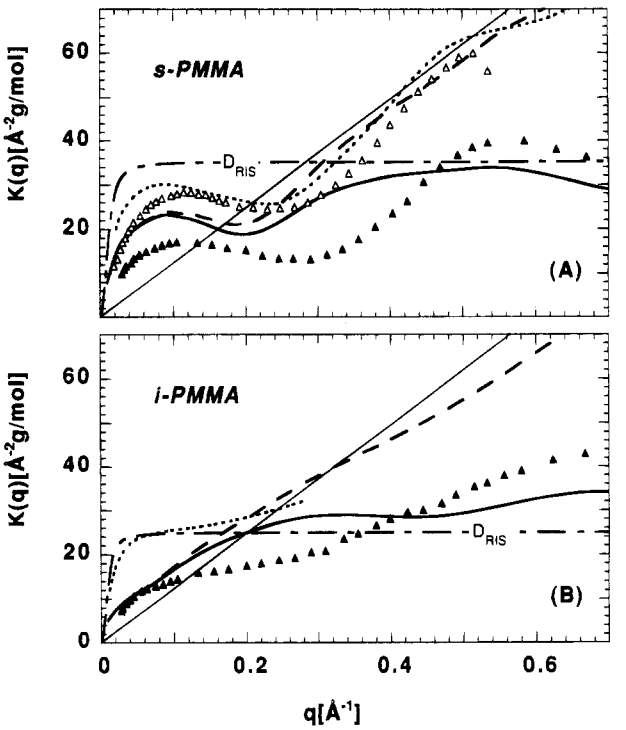

Figure 5. Kratky plots for s-PMMA (A) and i-PMMA (B). The solid and open triangles are experimental data from refs 5 and 6, respectively. Thick solid curves: MD simulation result using the f_i of ref 6. Dashed curves: MD simulation result using the C_α atoms only with $f_i = 1$. Dotted curves: six-state (s-PMMA) and two-state (i-PMMA) RIS models of refs 4 and 31. Thin solid lines: corresponding continuum limit for the straight chain. Dash-dashed curved: Kratky plot of the Debye function for the six-state RIS model of ref 4 (D_{RIS}); i.e., $\langle R_{2N}^2 \rangle$ in eq 7 is calculated based on the value of C_{2N} ($\approx C_\infty$) obtained in ref 4.

Figure 5 shows the simulated Kratky functions[30] defined by

$$K(q) = M_m N q^2 F(q) \qquad (5)$$

for the simulated s- and i-PMMA chains in comparison to experimental X-ray results[5,6] and theoretical results based on RIS model calculations.[4,31] Here $M_m = 100.1$ is the molecular weight of a monomer unit. Notice that the experimental data in Figure 5A are plotted exactly as given in the references and that the difference between them is largely due to a missing overall scale factor in one of the references, probably omitted when

the measured intensities where converted into $K(q)$. Qualitatively the MD result based on the form factors taken from ref 6 reproduces the experimental s-PMMA results quite well, including the maxima in the scattering function at $q \simeq 0.1$ and 0.55 Å^{-1}. Note that these q's roughly correspond to lengths of ~60 and ~10 Å, respectively, and the corresponding coiling, particularly for the smaller length, is clearly visible in Figure 2A. The RIS results, which are calculated based on scattering sites located at the positions of the C_α atoms only and using $f_i = 1$ for all sites, are, however, also quite good. Somewhat surprisingly the simulation results appear to perform better than the RIS calculations for small q, whereas for the larger q it appears that the reverse is true. Interestingly, if the scattering from the simulated high molecular weight fragments is calculated in the same fashion as for the RIS case, i.e., the scattering sites coincide with the C_α atoms and the corresponding $f_i = 1$, then the simulation results are quite close to the RIS results for $q \gtrsim 0.25$. Thus, it appears as if the modeling of the scattering sites within the monomer unit becomes important for $q \gtrsim 0.3$, so that discrepancies between simulation and experiment above $q \approx 0.3$ may be due to inaccuracies in the description of the form factors rather than being due to the conformational modeling. It is worth noting in this context that the authors of ref 6 have modeled the scattering of s-PMMA in benzene by a 14-state RIS model using the above excess form factors. Their theoretical result appears to fit the experimental data less accurately than either our simulation or the six-state RIS model results shown in Figure 5. It is also worth noting that very recently $F(q)$, was measured for s-PMMA in benzene by Yoshizaki et al.[32,33] These data, which we have not included explicitly in Figure 5A to not overcrowd this plot, exhibit a first maximum which is shifted to a somewhat larger q (~0.17 Å^{-1}) in comparison to the two data sets included in Figure 5A. In addition, the second maximum is suppressed to a mere shoulder and $F(q)$ increases monotonously. In the case of i-PMMA, as shown in Figure 5B, the RIS results are clearly qualitatively better than the simulation in the range $q \lesssim 0.3$, where the distribution of scattering sites within a monomer has only a small effect. The difference is mainly due to an additional broad maximum at $q \approx 0.2$ shown by the simulation result. Its occurrence is somewhat surprising, because the overall featureless shape of the experimental curve indicates a rather simple conformational behavior of i-PMMA. Notice that for comparison in Figure 5 we have included the Kratky functions for the two cases of a completely straight chain as well as for a Gaussian coil in the continuum limit. The scattering function of the former is simply given by

$$F(q) = \pi/qbN \tag{6}$$

where $b \approx 2.5$ Å is the monomer length calculated according to the values for the C−C bond length and the C−C_α−C angle given in Table 1, whereas the scattering function of the latter is given by the Debye function, i.e.

$$F(q) = \frac{2(e^{-x} + x - 1)}{x^2} \qquad x = \frac{1}{6}\langle R_{2N}^2\rangle q^2 \tag{7}$$

The corresponding Debye curves in Figure 5 (indicated by D_{RIS}) are calculated using $\langle R_{2N}^2\rangle \approx 2l^2NC_\infty$, where C_∞ is given by the six-state RIS values (cf. above).

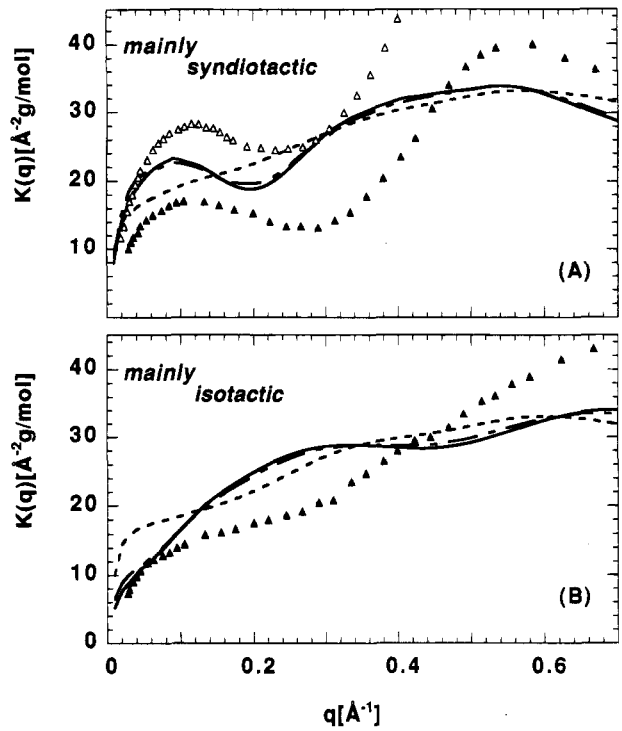

Figure 6. Kratky plots for the high molecular weight fragments with mixed tacticity. The solid and open triangles are the experimental data from refs 5 and 6, respectively. (A) Thick solid curves: simulation result using the f_i of ref 6 and $p_i = 0.0$. Long-short dashed curves: same as above but with $p_i = 0.1$. Short-dashed curves: same as above but with $p_i = 0.5$. (B) Same as part A but with p_i replaced by p_s.

Notice in particular that the long-wave length ($0.02 \lesssim q \lesssim 0.1$) scattering behavior of the experimental PMMA chains is not well described in terms of the scattering from Gaussian chains.

We can try to improve the agreement between simulation and experiment for i-PMMA following the idea that purely isotactic or purely syndiotactic polymer chains are not realistic, because the synthesis will yield polymer chains which are mainly isotactic but which may also contain syndiotactic segments. From Figure 2 it is intuitively plausible that the occurrence of mixed toxicity should effect the long- and intermediate-wavelength behavior of the scattering, i.e., the q region, where the disagreement is most severe. Unfortunately, here we do not have any information on the toxicity distribution within a polymer chain or within the polymer population. Thus in the following we discuss the results of simple model calculations, which should show the basic effects. Analogous to the construction procedure described above, we build high molecular weight fragments of mixed tacticity. However, instead of always connecting oligomers of the same tacticity as before, we now choose the oligomer conformation, which is to extend the chain, according to the probabilities p_s and p_i (where $p_s + p_i = 1$) from the respective syndiotactic or six-isotactic conformation lists. Thus, on average, each high molecular weight fragment constructed in this fashion consists of mp_s s-oligomer and mp_i i-oligomer segments, where m is the total number of segments in the fragment. As an aside, we remark that the direct simulation of an atactic oligomer is difficult due to the limited simulation box size, which, in turn, severely limits the statistical realization of atacticity. The scattering results for the high molecular weight fragments of mixed tacticity are shown in Figure 6. Part A shows the scattering from mainly syndiotactic

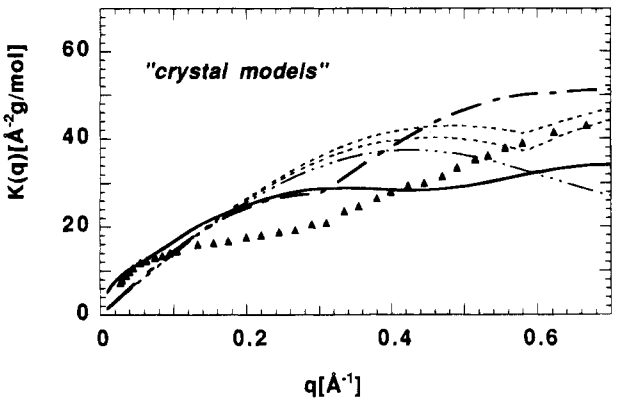

Figure 7. Kratky plots for single i-PMMA molecules consisting of 1000 monomers whose conformations are those of the 10/1 helix[11] (thick long–short-dashed line), the two 5/1 helices of ref 9 (thin dashed lines), and the 5/2 helix of ref 9 (long–short-dashed line). Again the symbols are the experimental data,[5] and the thick solid line is the simulation result using the form factors f_i of ref 6 (cf. Figure 5).

chains for the three cases when $p_i = 0.0$, 0.1, and 0.5. We see that only for $p_i = 0.5$ there is a pronounced effect, which, however, diminishes the agreement with the experiment. Part B shows the analogous plot for $p_s = 0.0$, 0.1, and 0.5 for the predominantly isotactic chains. Agains $p_s = 0.1$ deviates only slightly from $p_s = 0.0$, whereas $p_s = 0.5$, which significantly improves the qualitative agreement with the experimental data for $q \lesssim 0.3$, is too large to be realistic.

Finally, it is worth briefly discussing the Kratky plots, which one obtains for PMMA molecules in various crystal conformations, because there is always the question of how much of the crystal conformation can still be found in the short-wavelength region of the scattering function. Here we solely discuss i-PMMA for which several detailed suggestions for the crystal conformation can be found in the literature (cf. above). Figure 7 shows single-chain Kratky plots for the 10/1,[11] 5/1,[9] and 5/2[9] helices suggested for i-PMMA in the crystalline state. Interestingly, the 10/1 helix performs qualitatively quite well (except for $q \lesssim 0.1$). Furthermore, for $0.1 \lesssim q \lesssim 0.3$ the 10/1 helix is quite close to the simulation result. As the 10/1 helix is also our starting structure (cf. above), we cannot exclude the possibility that the discrepancies between simulation and experiment on the corresponding length scale are simply due to insufficient equilibration. Notice in this context that in the solid the 10/1 helix actually occurs as a double helix. Plotting the double-helix Kratky function (not shown here), however, yields a pronounced minimum at the large q values in Figure 7 and thus less good agrrement with the experimental results in comparison to the single 10/1 helix.

Polymer-Induced Solvent Structure

Finally, we briefly want to address the polymer-induced solvent structure and its dependence on tacticity based on the radial distribution functions $g_{cm}(r_a)$ defined by

$$g_{cm}(r_a) = \frac{\langle \varrho_{cm}(r_a) \rangle}{\varrho_{cm}} \tag{8}$$

Here $\varrho_{cm}(r_a)$ denotes the number density of benzene molecules, whose center of mass distance from an atom of type a in the polymer is r_a. ϱ_{cm} is the bulk center of mass density of benzene. The average is over all atoms

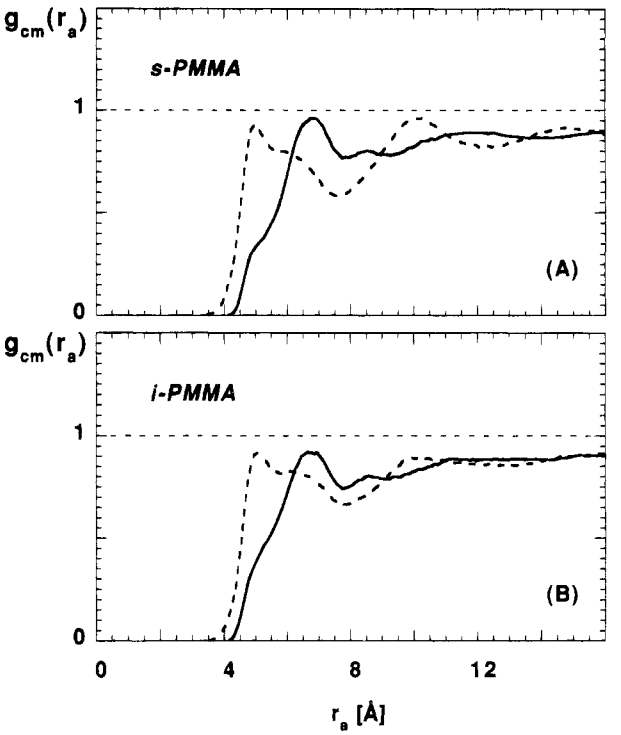

Figure 8. Radial benzene distribution function $g_{cm}(r_a)$ for s- (A) and i-PMMA (B). Here r_a denotes the benzene center of mass–C_α separation (solid lines) and the benzene center of mass–O_{ester} separation (dashed lines), respectively.

of type a and time. Figure 8 shows $g_{cm}(r_a)$, when a denotes the C_α carbon atom and the ester oxygen, respectively. For both s- and i-PMMA the range of the solvent-induced structure, i.e., the effective diameter of the polymer cross section, is about 10–12 Å, where the spacing of the major density peaks is determined by the size of the solvent molecule. Note that the corresponding sets of curves for s- and i-PMMA are similar, except that the structure of g_{ester} is more pronounced in the syndiotactic case. Notice also that here $g_{cm}(r_a)$ does not approach unity within the range shown, because of solvent exclusion due to the PMMA segment itself. Finally, it is worth noting that the polymer-induced solvation structure, i.e., the attending variation in the electron density, might be important in calculating the scattering behavior in the range where $q \gtrsim 0.3$. This is a possibility which we want to investigate more carefully in future work.

Conclusion

In this work we have carried out molecular dynamics simulations of syndio- and isotactic oligomers of PMMA in explicit benzene, using a standard force field with tabulated parameters. By connecting time-uncorrelated oligomer conformations, we construct high molecular weight fragments corresponding to experimental molecular weights. For s-PMMA our approach semiquantitatively reproduces the experimental X-ray scattering results obtained on dilute solutions, whereas for i-PMMA the agreement is not so good. Overall, however, our MD simulation, with the parameter taken from a standard data base with no further refinement, describes the scattering behavior of the system almost as well as the rather complicated and over the years refined RIS models. In addition, it appears that the treatment of the scattering within a monomer plays a significant role for the proper description of the experimental data in the q-range considered here.

Acknowledgment. The authors acknowledge several useful discussions with Prof. G. Wegner and Prof. R. Kirste during the course of this work.

References and Notes

(1) Weiner, S. J.; Kollman, P. A.; Nguyen, D. T.; Case, D. A. *J. Comput. Chem.* **1986**, *7*, 230.
(2) Weiner, S. J.; Kollman, P. A.; Case, D. A.; Chandra Singh, U.; Ghio, C.; Alagona, G.; Profeta, S., Jr.; Weiner, P. *J. Am. Chem. Soc.* **1984**, *106*, 765.
(3) Helfrich, J.; Hentschke, R.; Apel, U. M. *Macromolecules* **1994**, *27*, 472.
(4) Vacatello, M.; Flory, P. J. *Macromolecules* **1986**, *19*, 405.
(5) Kirste, P. G.; Oberthür, R. C. In *Small Angle X-ray Scattering*; Glatter, O., Kratky, O., Eds.; 1982; p 427. (Notice that erroneously in this reference acetone is mentioned as solvent instead of benzene.)
(6) Yamaguchi, S.; Hayashi, H.; Hamada, F.; Nakajima, A. *Macromolecules* **1984**, *17*, 2131.
(7) Kusuyama, H.; Takase, M.; Higashihata, Y.; Hsiung-To, T.; Chatani, Y.; Tadokoro, H. *Polymer* **1982**, *23*, 1256.
(8) Kusuyama, H.; H.; Miyamoto, M.; Chatani, Y.; Tadokoro, H. *Polym. Commun.* **1983**, *24*, 119.
(9) Tadokoro, H.; Chatani, Y.; Kusanagi, H.; Yokoyama, M. *Macromolecules* **1970**, *3*, 441.
(10) Tadokoro, H.; Tai, K.; Yokoyama, M.; Kobayashi, M. *J. Polym. Sci., Polym. Phys. Ed.* **1973**, *11*, 825.
(11) Tadokoro, H. *Macromolecules* **1976**, *9*, 531.
(12) Bosscher, F.; ten Brinke, G.; Eshuis, A.; Challa, G. *Macromolecules* **1982**, *15*, 1364.
(13) POLYGRAF, Version 3.0, Molecular Simulations, Inc., 1992.
(14) Depner, M. Computersimulationen von Modellen einzelner realistischer Polymerketten. Dissertation, Johannes Gutenberg Universität, Mainz, Germany, 1991.
(15) Allen, M. P.; Tildesley, D. J. *Computer Simulations of Liquids*; Oxford University Press: Oxford, U.K., 1992.
(16) Charifson, P. S.; Hiskey, R. G.; Pedersen, L. G. *J. Comput. Chem.* **1990**, *11*, 1181.
(17) Rappé, A. K.; Goddard, W. A. *J. Phys. Chem.* **1991**, *95*, 3358.
(18) Karlström, G.; Linse, P.; Wallquist, A.; Jönsson, B. *J. Am. Chem. Soc.* **1983**, *105*, 3777.
(19) Berendsen, H. J. C.; Postma, J. P. M.; van Gunsteren, W. F.; Di Nola, A.; Haak, J. R. *J. Phys. Chem.* **1984**, *81*, 3684.
(20) Jenkins, R.; Porter, R. S. *Polymer* **1982**, *23*, 105.
(21) Yamakawa, H. In *Modern Theory of Polymer Solutions*; Harper and Row: New York, 1971.
(22) Sakurada, I.; Nkajima, A.; Yoshizaki, O.; Nakamae, K. *Kolloid Z.* **1962**, *186*, 41.
(23) Schulz, G. V.; Wunderlich, W.; Kirste, R. *Makromol. Chem.* **1964**, *75*, 22.
(24) Krause, S.; Cohn-Ginsberg, E. J. *J. Phys. Chem.* **1963**, *67*, 1479.
(25) Vadusewan, P.; Santappa, M. J. *J. Polym. Sci., Polym. Phys. Ed.* **1971**, *9*, 482.
(26) Chinai, S. N.; Valles, R. J. *J. Polym. Sci.* **1959**, *39*, 363.
(27) Fox, T. G. *Polymer* **1962**, *3*, 111.
(28) *Polymer Handbook*, 3rd ed.; Brandrup, J., Immergut, E. H., Eds.; John Wiley & Sons: New York, 1989.
(29) de Gennes, P.-G. *Scaling Concepts in Polymer Physics*; Cornell University Press: New York, 1979.
(30) Flory, P. J. *Statistical Mechanics of Chain Molecules*; Hanser: New York, 1988.
(31) Yoon, D. Y.; Flory, P. J. *Polymer* **1975**, *16*, 645.
(32) Yoshizaki, T.; Hayashi, H.; Yamakwa, H. *Macromolecules* **1993**, *26*, 4037.
(33) Yoshizaki, T.; Hayashi, H.; Yamakawa, H. *Macromolecules* **1994**, *27*, 4259.

MA941318C